

Contents lists available at ScienceDirect

Chemosphere

journal homepage: www.elsevier.com/locate/chemosphere



Decomposition of dimethyl methylphosphonate vapor on ultrathin-film titania photocatalytic light absorber



Wei Wu ^a, Haomin Song ^b, Qiaoqiang Gan ^{b, **}, Dongxia Liu ^{a, *}

- ^a Department of Chemical and Biomolecular Engineering, University of Maryland, College Park, MD, 20742, USA
- b Department of Electrical Engineering, The State University of New York at Buffalo, Buffalo, NY 14260, USA

HIGHLIGHTS

- Photocatalytic decomposition of DMMP vapor was studied on thin film TiO2 UFPLA.
- Light absorption boosted by UFPLA promotes catalytic activity of TiO₂ thin films.
- DMMP decomposition rate is increased >2000 times compared to that on Aeroxide®P25.
- Kinetic data of DMMP decomposition is described by Langmuir-Hinshelwood model.

ARTICLE INFO

Article history: Received 27 August 2020 Received in revised form 14 January 2021 Accepted 17 January 2021 Available online 23 January 2021

Handling Editor: Jun Huang

Keywords: Ultrathin-film light absorber Titania Organophosphorus Chemical war agent Photocatalytic decomposition Nanocavity

ABSTRACT

The decomposition of chemical warfare agent simulant, dimethyl methylphophonate (DMMP) vapor, was investigated on an ultrathin film titania (TiO₂) photocatalytic light absorber. The light absorber contains an aluminum (Al) reflector and the TiO₂ thin film with different thicknesses, sequentially deposited on a supportive glass substrate. The designed structure constructs a nanocavity that exhibits strong light absorption within the photocatalytic TiO₂ ultrathin film. Thus, the intrinsic trade-off between optical absorption and charge carrier extraction efficiency, i.e., a light absorber should be thick enough to absorb the light allowable by its band gap but thin enough to allow charge carrier extraction for catalytic reactions, is conquered. The TiO₂/Al light absorber significantly boosted TiO₂ photocatalytic activity compared to the benchmark Aeroxide®P25 catalyst (i.e., up to 2013 times increase in reaction rate). The effects of reactant (i.e. DMMP, water and oxygen, respectively) partial pressure and reaction temperature on photocatalytic decomposition of DMMP by the ultrathin-film TiO₂ photocatalytic light absorber were studied. Kinetic data of the DMMP decomposition can be described by the Langmuir-Hinshelwood model.

© 2021 Elsevier Ltd. All rights reserved.

1. Introduction

Security threat by possible use of chemical war agents (CWAs) by terrorists or in battlefield, and environmental pollution by industrial toxic chemicals have been growing global concerns (Knudson, 2001; Alexander and Klein, 2006; MatouŠEk, 2006; Tetyana et al., 2006; Talmage et al., 2007). Photocatalytic detoxification using solar energy represents an environmentally friendly and cost-efficient strategy to degrade these toxic chemicals (Kabra et al., 2004; Robertson et al., 2005; Blanco-Galvez et al., 2006;

E-mail addresses: qqgan@buffalo.edu (Q. Gan), liud@umd.edu (D. Liu).

Dalrymple et al., 2010; Thakur et al., 2010; Ahmed and Haider, 2018). Titania (TiO_2) has been the most frequently employed photocatalyst in detoxification processes due to its inherent environmental friendliness and low-cost, together with the potential of complete mineralization of organic toxic chemicals. The current photocatalytic processes, however, are highly inefficient, particularly in the case of solar activation. This inefficiency arises because the charge carrier (electrons/holes, e^-/h^+) extraction efficiency in photocatalysts is far too low (Kitano et al., 2007; Habisreutinger et al., 2013; Liu and Chen, 2014; Ma et al., 2014). The charge carriers are generated by light irradiation to initiate the catalytic reactions, but their recombination rates are much faster than utilization, which highly limits the activity of photocatalysts. Catalyst materials and design strategies that have potential to enhance e^-/h^+ extraction efficiency, light absorption, and the

^{*} Corresponding author.

^{**} Corresponding author.

resultant catalytic activity and efficiency in photocatalytic detoxification are highly desired.

Nanostructured TiO2-based catalysts such as nanowires, nanotubes or nanosheets (Mor et al., 2006; Kamat, 2007; Jun et al., 2012; Liang et al., 2012; Liu et al., 2015) have been studied to promote efficiency in photocatalysis. The nano-sized TiO₂ catalysts shorten the diffusion length, disfavor the electron and hole recombination and enhance multi-electron transfer for photocatalytic reactions (Linsebigler et al., 1995; Aprile et al., 2008; Fujishima et al., 2008). Although an enhancement in catalytic performance of nanostructured TiO2-based materials has been observed, the photocatalytic efficiency is still too low to meet practical applications, mainly due to lack of sufficient light adsorption in nanostructured photocatalyst materials. The decrease in catalyst particle size leads to a significant reduction in light absorption and generation of charger carriers. The intrinsic trade-off between optical absorption and charge carrier extraction efficiency, i.e., a light absorber should be thick enough to absorb the light allowable by its band gap but thin enough to allow charge carrier extraction for catalytic reactions, therefore, will be conquered.

One promising scheme to enhance the optical absorption without sacrificing the catalytic activity/selectivity in nanostructured catalysts would be to employ ultra-thin film super light absorbers on the catalysts. For instance, planar thin film interference can enhance the optical absorption within ultra-thin films (Dotan et al., 2013; Kats et al., 2013). This mechanism could significantly reduce the required thickness of the light absorbers. For instance, over 60% resonance absorption was successfully demonstrated with a 1.5-nm-thick Ge film (Song et al., 2014) and even a monolayer of MoS₂(Janisch et al., 2016) on predesigned nanocavities, paving the way for high-efficiency ultrathin-film energy conversion materials, structures and devices (Xia et al., 2017), including photocatalytic systems. In particular, the boosted optical absorption in planar ultra-thin photocatalytic Ti-doped α-Fe₂O₃ films (e.g. ~26 nm) was successfully used for efficient water splitting (Dotan et al., 2013). Our previous work has designed the ultrathin-film photocatalytic light absorber (UFPLA), made by sequential deposition of an aluminum (Al) reflector and a TiO₂ thin film (<30 nm) on a glass substrate, which is effective to resolve the intrinsic trade-off between optical absorption and charge carrier extraction efficiency. The TiO₂/Al films introduced the active sites, and manipulated the phase of the reflective partial waves to realize the destructive interference. Therefore, the light absorption capability of the TiO₂ thin film was maximized, significantly increasing catalytic efficiency by generating much more surface charge carriers. For example, the UFPLA structures significantly improve activity and selectivity in photocatalytic carbon dioxide (CO₂) reduction with water to oxygenated hydrocarbons (Song et al., 2018). In comparison to the benchmark photocatalyst (Aeroxide®P25), the CO₂ reduction rate was enhanced up to a factor of 1145 times (Song et al., 2018).

In this work, we employed the UFPLA structures with TiO_2 thin-films for the photocatalytic detoxification of CWAs. Due to toxicity of CWAs, the dimethyl methylphophonate (DMMP) was used as the simulant in this study. The performance of UFPLA with different TiO_2 film thicknesses in photocatalytic decomposition of DMMP vapor was studied and compared to that of Aeroxide®P25 catalyst. The effects of reactant (i.e. DMMP, water and oxygen, respectively) partial pressure and reaction temperature on DMMP decomposition were measured. The kinetic data were described by both Langmuir-Hinshelwood and Elay-Redial models, and the former gave a better fitting.

2. Experimental

2.1. Materials

Dimethyl methylphosphonate (DMMP, 97% purity) and Aeroxide® P25 were purchased from Alfa Aesar. Air (ultrapure), nitrogen (N_2 , ultrapure) Argon (Ar, ultrapure) and helium (He, ultrapure) were purchased from Airgas. Deionized (DI) water (H_2O) was used throughout the experiments.

2.2. UFPLA preparation

The UFPLA, comprised of an Al reflector and a TiO₂ thin film, was synthesized using the method reported in our previous work (Song et al., 2018). Typically, the Al reflector layer (150-nm thick) was deposited on a glass substrate using the Al pellets (99.999%, EVMAL50QXQ-D, Kurt J. Lesker) in the Kurt J. Lesker AXXIS electron beam evaporator. The pressure in the evaporator chamber during Al deposition was controlled at 5×10^{-7} Torr. A flow benchtop reactor (FlexAL, Oxford Instruments) was used to prepare the TiO2 thinfilm layers in the UFPLA via the atomic layer deposition (ALD) process. The ALD of TiO₂ was conducted by alternative exposure to titanium isopropoxide (i.e., TTIP, Japan Advanced Chemicals) for 1.5 s and DI water at 473 K for 3.5 s, followed by Ar purge for 1.5 s after each exposure. Each ALD cycle would result in 0.05-nm-thick TiO₂ deposition. Figure S3 in the Supporting Information shows the schematic of the ultrathin-film TiO₂ photocatalytic light absorber preparation process.

2.3. Photocatalytic tests

The photocatalytic DMMP decomposition was tested in the experimental set-up shown in Fig. 1. A homemade cylindrical reactor, as illustrated in our previous publication (Song et al., 2018), was used to hold the UFPLA structure and the catalytic reaction. The reactor consists of a stainless steel body and two quartz windows of 50 mm in diameter and 5 mm in thickness. The internal volume of the batch reactor is 14.1 cm³. Two gas connection lines (inlet and outlet of the reactor) stay opposite to each other on the perimeter wall of the cylindrical photocatalytic reactor body. The reactor was wrapped with heating tape to control the reaction temperature.

In a typical experiment, after the UFPLA was placed inside the reactor, the DMMP vapor was introduced by a He flow $(0.17 \text{ cm}^3 \text{ s}^{-1})$ through a DMMP bubbler. Similarly, the water vapor was introduced by an air flow (0.67 cm³ s⁻¹) through a water bubbler. Nitrogen (N2) was used as a balance gas in all the experiments. The gas mixture was kept flowing through the reactor for 1.5 h to flush the system and reach stable DMMP, H₂O and air (i.e. oxygen, O2) compositions. Then, both the inlet and outlet of the reactor in Fig. 1 were closed, and the xenon (Xe) light irradiation (OSRAM XBO 450 W PFR) was applied onto the top window of the reactor. After 5-h irradiation, the Xe lamp was turned off and the gas mixture in the reactor was carried out by a N2 flow at $0.37 \, \text{cm}^3 \, \text{s}^{-1}$ for $0.5 \, \text{h}$. The isopropanol trap in the experimental setup was used to collect DMMP residue and all products in the reaction. An aliquot of isopropanol solution in the trap was traced by a gas chromatography (Agilent Technologies, 7890 A) equipped with methylsiloxane capillary column 50.0 m \times 320 $\mu m \times$ 0.52 $\mu m)$ connected to a flame ionization detector (FID) for composition analysis. For comparison purpose, the photocatalytic DMMP decomposition was run in the reactor charged with 50 mg commercial Aeroxide®P25 catalyst, which was

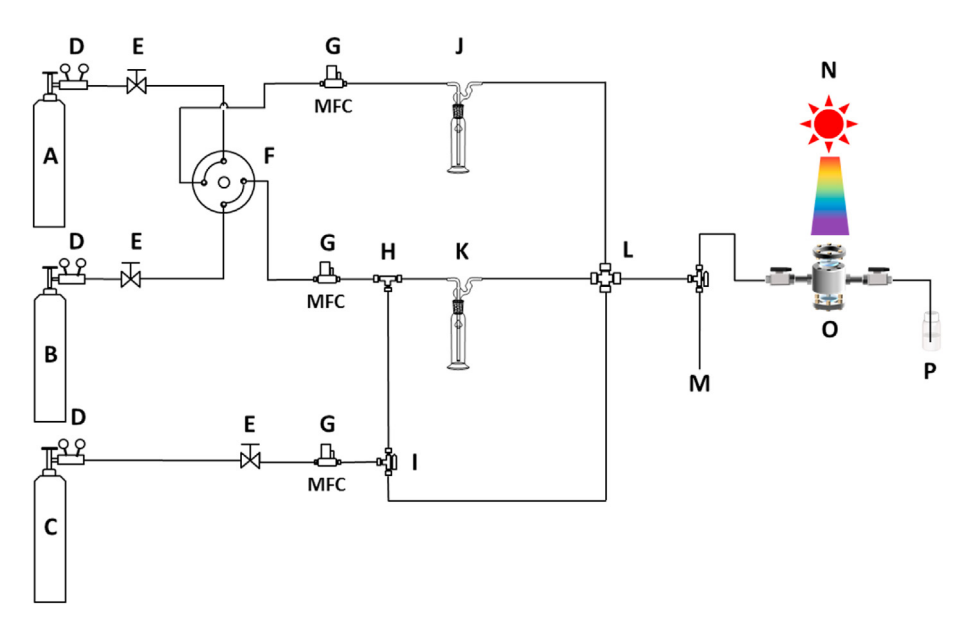


Fig. 1. Schematic diagram of the reaction system [A: helium cylinder, B: air cylinder, C: nitrogen cylinder, D: cylinder regulator, E: shut-off valve, F: Valco 4-way valve, G: mass flow controller, H: union tee connector, I: 3-way valve, J: DMMP in bubbler, K: water in bubbler, L: union cross, M: flowmeter, N: 450 W xenon lamp, O: photocatalytic reactor, P: isopropanol trap].

compressed into a thin film with the same geometric surface area as that of the TiO_2 film in the UFPLA.

3. Results and discussion

3.1. Structure and optical absorption of UFPLA structures

The physicochemical property of TiO_2 thin film in TiO_2/Al UFPLA structures as well as the Aeroxide®P25 control sample have been examined and the results was described in detail in our previous publication (Song et al., 2018). For completeness, we provide a brief discussion here and the characterization data are presented in Section S1 in the Supporting Information. The surface of TiO_2 thin film is uniform, following the pattern of Al layer, independent on the TiO_2 film thickness (Figure S1a-b). X-ray diffraction (XRD) measurement shows that both TiO_2 and Al are in amorphous form since only the diffraction peak of the glass substrate (i.e., $2\theta = 22.9^\circ$) was observed (Figure S1c).

Fig. 2a shows the general principle of the TiO_2/Al UFPLA used in the photocatalytic decomposition of DMMP. The UFPLA is designed based on the thin-film interferometer constructed by a TiO_2 film on a highly reflective Al film. Since the Al layer is highly reflective, no light is transmitted through the UFPLA. Instead, the light is

reflected back and forth at the air/TiO₂ and TiO₂/Al interfaces. Specifically, when light reaches the top air/TiO₂ interface, part of this incident light will be reflected back to air, which is denoted as r_1 in Fig. 2a. The other part of the incident light is transmitted into the TiO₂ film, propagates until it is reflected by the bottom TiO₂/Al interface, and continue to propagate to the air/TiO₂ interface. At this interface, the light is divided into two parts again. One part exits back to air, which is denoted as r'_1 in Fig. 2a. The rest of the light repeats the previous process and bounces back and forth between the air/TiO2 and TiO2/Al interfaces. The following partial waves transmitted back to air are denoted as r_1'' , r_1''' , r_1'''' , etc. Except for the first partial wave, all other partial waves propagate in the TiO₂ layer at least one round-trip. Light propagation results in phase change of light, which can be determined by the thickness of the TiO₂ film. Thus, in order to enhance the light harvesting capability of UFPLAs, we can intentionally tune the thickness of the TiO₂ film to create destructive interference among these partial waves, leading to a complete suppression of total reflection, i.e., perfect absorption. Fig. 2b indicates the modeled optical absorption of the UFPLA at each wavelength from 210 nm to 450 nm as the function of the thickness of TiO2 films. The results were simulated by Fresnel equation (see more details of the modeling in Section S1 in the

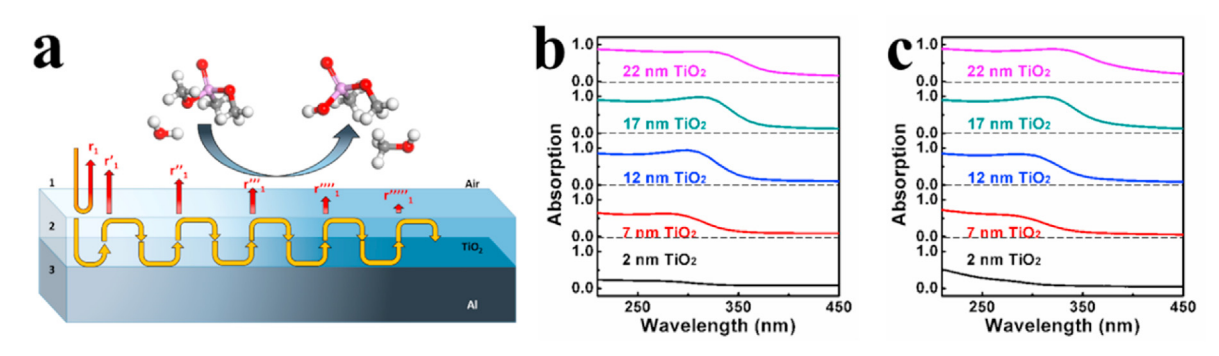


Fig. 2. Schematic of the two-layered TiO₂/Al UFPLA structure (a). Modeled (b) and measured (c) optical light absorption as a function of the thickness of TiO₂ films in the TiO₂/Al UFPLA.

Supporting Information). It can be seen that strong resonant absorption peaks over 90% from 270 nm to 325 nm can be obtained in the optimized TiO₂ film thickness region of 12–19 nm. Beyond this range, the overall absorption will decrease with thinner or thicker TiO₂ layers. In order to validate this theoretical prediction, we measured the optical absorption spectra of the UFPLA structures with TiO₂ thickness varied from 2, 7, 12, 17–22 nm in sequence, as shown in Fig. 2c. The increase in thickness of TiO₂ layer enhances and then suppresses the optical absorption of the entire UFPLA structures. The obvious peak resonant absorption over 90% from 270 nm to 325 nm can be obtained in the optimized TiO₂ film thickness region of 12–17 nm. At the optimized TiO₂ film thickness, the super strong optical absorption was realized, agreeing well with the theoretical prediction shown in Fig. 2b.

3.2. DMMP decomposition over UFPLA structures

To verify effectiveness of the UFPLA structure in photocatalytic decomposition of DMMP, two control experiments were carried out first. In one case, the DMMP was exposed to the UFPLA that is comprised of 12-nm-TiO₂ thin-film in the absence of light irradiation (i.e. darkness condition). After 5 h reaction time, without light irradiation, the DMMP decomposition was 0.6%. In the other case, the UFPLA structure was absent in the reactor (i.e., only glass slide was used) and the light irradiation was applied for 5 h onto DMMP. The DMMP decomposition was 0.7%, close to the conversion tested in the first case. The products from DMMP decomposition include intermediates such as methylphosphonic acid and formic acid as well as the end products of carbon dioxide, water and phosphate. Both control experiments indicate that the photocatalytic decomposition DMMP requires for presence of both the UFPLA structure and light irradiation, which means that the decomposition is the result of photo-excited TiO2 catalysis and not direct photolysis or ground state TiO₂ catalyzed reactions. In the following sections, we studied the effectiveness of UFPLA in DMMP decomposition, in comparison to Aeroxide®P25, and effects of TiO2 thin-film thickness in the UFPLA on the reaction.

3.2.1. Effectiveness of UFPLA for photocatalytic DMMP decomposition

Fig. 3a shows the photocatalytic DMMP decomposition over both UFPLA that has 12-nm-TiO₂ thin-film (i.e. thickness of TiO₂ thin-film is 12 nm) and Aeroxide®P25 catalysts as a function of

reaction time. With increasing reaction time (or light irradiation time), DMMP decomposition increases. Overall, the UFPLA structure has higher DMMP decomposition than the Aeroxide®P25 catalyst. It should be noted that the employed UFPLA has a circular shape with a dimension of 30 mm in diameter. By considering the 12 nm thickness of TiO₂ thin-film in the UFPLA and density of TiO₂ of 4.23 g cm⁻³ (Mergel, 2001; Kusior et al., 2013; Song et al., 2018), the mass of TiO₂ catalyst in the UFPLA is 3.59×10^{-5} g, calculated by the product of TiO₂ thin-film geometric surface area, thickness and density. As noted in the experimental section, 0.05 g Aeroxide®P25 was used in the test. If we use the DMMP conversion data collected at 5 h of reaction to evaluate the rate of DMMP decomposition per Ti site in both materials, 6.08 and 3.02×10^{-3} mol [mol Ti]⁻¹ s⁻¹ are obtained, respectively. This indicates that the TiO₂ catalyst in the UFPLA structure has a 2013-fold enhancement in activity in photocatalytic decomposition of DMMP. The increase in TiO₂ activity in the UFPLA should be attributed to the boosted optical absorption as discussed above.

3.2.2. Effects of TiO2 thin-film thickness in UFPLA

The thickness of TiO₂ thin films in the UFPLA influences the light absorption, as indicated in Fig. 2b. To understand how the change in light absorption affects the photocatalytic DMMP decomposition, we employed the UFPLAs with TiO₂ thin-film thicknesses of 2, 7, 12, 17 and 22 nm, respectively, in the tests. After 5 h reaction, the DMMP decomposition increased from 1.1%, 3.2%-9.2%, and then decreased to 5.1% and 3.3%, as shown in Fig. 3b. The trend of increase and then decrease in DMMP decomposition with respect to increasing TiO₂ film thickness in the UFPLA structures is consistent with that of the optical absorption of the nanocavity in Fig. 2b. The mismatch between the maximum light absorption (i.e. occurring on 17-nm-TiO₂) and the highest DMMP decomposition (i.e. on 12nm-TiO₂) in the UFPLAs indicated that the light absorption is not the sole factor dominating the photocatalytic decomposition when the TiO₂ film is thick. This discrepancy has also been observed in our previous work (Song et al., 2018).

The DMMP decomposition rate over each UFPLA was further analyzed and compared to that of Aeroxide®P25 to understand the effects of TiO₂ thin-film thickness. The results were summarized in Fig. 3c and Table S1. In all cases, the UFPLA catalysts exhibited more than 2 orders of magnitude enhancement in DMMP decomposition rate compared to the Aeroxide®P25 catalyst. This indicates the remarkable contribution of optical absorption by the nanocavity

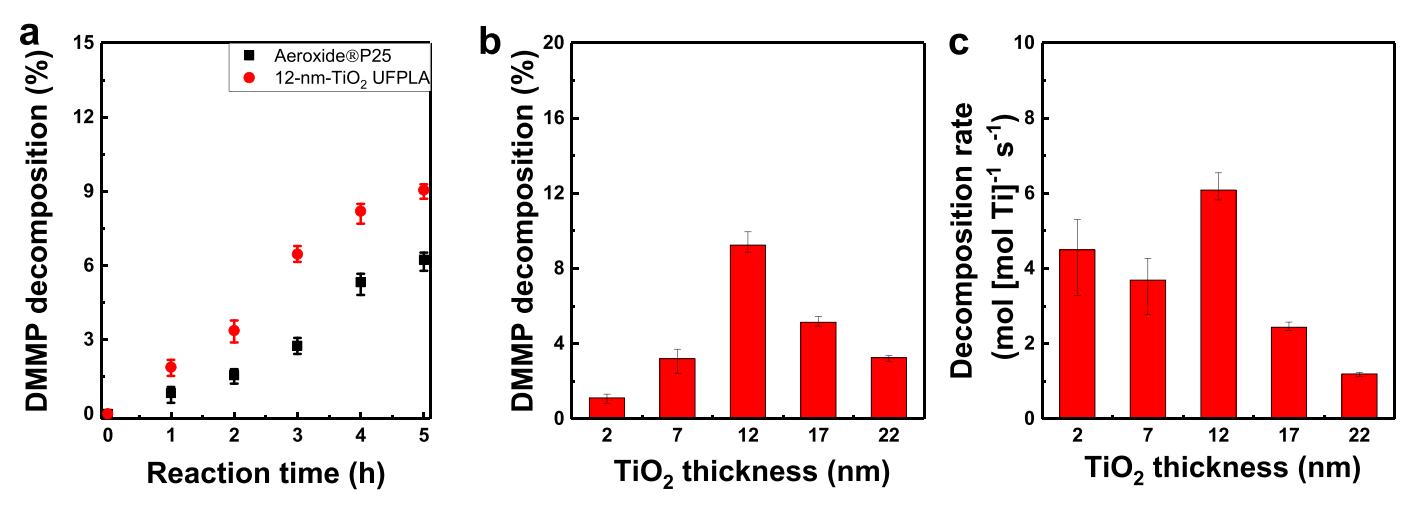


Fig. 3. DMMP decomposition over 12-nm-TiO₂ UFPLA and Aeroxide®P25 as a function of reaction time (a), DMMP decomposition as a function of TiO₂ film thickness in UFPLA structures after 5 h irradiation (b) and DMMP decomposition rate as a function of TiO₂ film thickness in UFPLA structures (c). (Reaction conditions: 333 K, 7.09 Pa DMMP pressure, 1.19 kPa H₂O pressure, 17.02 kPa O₂ pressure, 5 h reaction time.)

structure in UFPLA to the photocatalytic reaction. With an increase in the thickness of the TiO_2 thin film in the UFPLA structure, the decomposition rate decreases except for the UFPLA with 12-nm- TiO_2 thin-film. This pattern demonstrates that the activity of individual Ti-sites is influenced by the thickness of TiO_2 film and the related site environment.

The DMMP decomposition rate is closely correlated to synergetic effect between the optical absorption intensity and charge carrier lifetime in UFPLAs (Song et al., 2018). As explored in our previous work (Song et al., 2018), when the TiO₂ film is thin, in the cases of the 2 and 7-nm-TiO₂ UFPLAs, the photogenerated carriers within TiO₂ film have a longer lifetime and consequently have a higher probability to participate the photocatalytic DMMP decomposition. However, the relative weak light harvesting capabilities, as shown in Fig. 2b, on these two samples hindered the charge carrier generation. As a result, both UFPLA structures reflected a high DMMP decomposition rate, but did not reach the summit. When the thickness of the TiO2 film in the UFPLA is increased to 12 nm, the slightly suppressed charge carrier lifetime and moderately enhanced light absorption capability (Song et al., 2018) promote the synergetic effect. Consequently, the 12-nm-TiO₂ UFPLA exhibited a highest DMMP decomposition rate at 6.08 mol [mol Ti] $^{-1}$ s $^{-1}$. As the TiO₂ film thickness increases to 17 and 22 nm, although the light absorption reaches maximum capability, the steeply reduction in lifetime of charge carriers (Song et al., 2018) retards the catalytic performance in DMMP decomposition. Thus, lower DMMP decomposition rates were observed on both 17 and 22-nm-TiO₂ UFPLA catalysts. The apparent quantum efficiency, defined as the ratio of the global rate of DMMP decomposition to the total energy emitted from the light source, was calculated for all the UFPLAs. As shown in Table S1, the apparent quantum efficiency increases and then decreases with increasing TiO₂ layer thickness in the UFPLAs. The synergy of light absorption and charge carrier lifetime was maximized in the UFPLA with 12 nm TiO₂ thickness which enabled the highest quantum efficiency.

3.3. Kinetic modelling of DMMP photocatalytic decomposition over UFPLA catalyst

Photocatalytic decomposition of organophosphonic acid compounds over TiO₂ catalysts have been previously reported (Grätzel et al., 1990; Mengyue et al., 1995; Konstantinou et al., 2001;

Hirakawa and Nosaka, 2002; Echavia et al., 2009). The complete reaction mechanism is too complex to conclude until now. However, the general understanding on the reaction initiation is the photoexcitation of TiO2 by light irradiation (hv) generates an electron-hole $(e_c^--h_v^+)$ pair $(TiO_2 + hv \rightarrow e_c^- + h_v^+)$ in the conduction and valence bands, respectively (Kumar and Devi, 2011; Lan et al., 2013; Schneider et al., 2014; Fagan et al., 2016; Liu et al., 2017). The conduction band electron is believed to react with adsorbed oxygen (O_2) to form a superoxide ion $(e_c^- + O_2 \rightarrow O_2^-)$. The valence band hole might react with adsorbed water (H2O) to form hydroxyl radicals $(h_v^+ + H_2O \rightarrow H^+ + OH \cdot)$. The subsequent reactions of adsorbed hydroxyl radicals are regarded as the predominant degradation pathways of organophosphonic acid compounds. Apparently, three reactant compounds, DMMP, H₂O and O₂ are all involved, at some degrees, in the DMMP decomposition process. The DMMP decomposition on the UFPLA structure has not been researched before. Therefore, in this section, we aimed to understand the kinetics of DMMP decomposition and its dependence on the reactant pressures over the UFPLA structure, as well as verify the models that can fit the measured kinetics in this new catalytic optical absorber structures.

3.3.1. Dependence of DMMP decomposition on DMMP, H_2O or O_2 reactant

To investigate the dependence of DMMP decomposition on the concentration of DMMP, H_2O or O_2 occurring in UFPLA structure, the decomposition rate of DMMP as a function of partial pressure of each reactant was examined at 333 K (Fig. 4). It should be noted that we focused on the kinetics of DMMP decomposition on the UFPLA containing 12-nm- TiO_2 thin-film since it showed the best performance as discussed in Section 3.2. The initial decomposition rates were determined from the first 10% disappearance of the starting reactant to minimize the effects of products on the initial kinetics.

Fig. 4a shows the DMMP decomposition rate increases rapidly with increasing DMMP partial pressure (p_{DMMP}) in the beginning. When p_{DMMP} is high, the decomposition rate reaches a plateau. Overall, the dependence follows the Langmuir behavior. The dependence of DMMP decomposition rate on the partial pressure of water (p_{H_2O}) is similar to that of dependence on p_{DMMP} (Fig. 4b). Fig. 4c shows the correlation between the DMMP decomposition rate and partial pressure of O_2 (p_{O_2}) in the reactor. Different from the first two cases, the rate does not show any obvious dependence

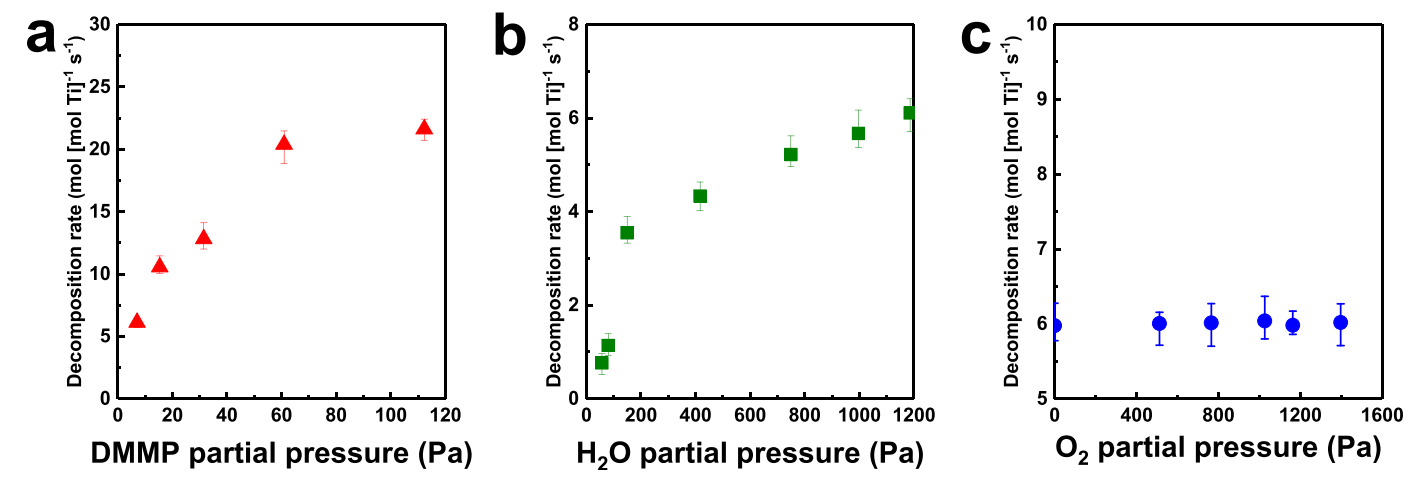


Fig. 4. Measured DMMP decomposition rate as a function of DMMP pressure (a), H₂O partial pressure (b) and O₂ pressure (c) over 12-nm-TiO₂ UFPLA at 333 K (Reaction conditions in Fig. 4a: 1.19 kPa H₂O pressure, 17.02 kPa O₂ pressure, 5 h reaction time; Reaction conditions in Fig. 4b: 7.09 Pa DMMP pressure, 4.28 kPa O₂ pressure, 5 h reaction time; Reaction conditions in Fig. 4c: 7.09 Pa DMMP pressure, 1.19 kPa H₂O pressure, 5 h reaction time.).

Step (1): DMMP +
$$* \stackrel{K_1}{\leftrightarrow}$$
 DMMP*
Step (2): $H_2O + * \stackrel{K_2}{\leftrightarrow}$ H_2O^*
Step (3): DMMP* + $H_2O^* \stackrel{k_3}{\rightarrow}$ MMP* + CH_3OH (RLS)
Step (4): MMP* $\stackrel{K_4}{\leftrightarrow}$ MMP + $*$

Scheme 1. Elementary steps in Langmuir-Hinshelwood model in photocatalytic DMMP decomposition.

on p_{0_2} , even when p_{0_2} is very low. This phenomenon is consistent with the previous report (De Laat et al., 2010) that shows the oxygen does not attend the initial steps in main reaction pathway. However, the trace amount of O_2 residue or O_2 impurity in the reactor might be enough to contribute to the decomposition reactions.

3.3.2. Kinetics modelling for DMMP decomposition

Despite the complex mechanisms of photocatalytic organophosphonate acid decomposition, simple kinetic models still have been used to interpret observed kinetics (Krosley et al., 1993; O'Shea et al., 1997; Obee and Satyapal, 1998; Kozlova et al., 2004; Moss et al., 2005). Among different models, the most common ones are Langmuir-Hinshelwood and Eley-Rideal models. Therefore, we simply explored both models for the kinetics analysis, aiming to interpret the collected kinetics data and to obtain initial kinetic parameters to guide further understanding on DMMP decomposition behavior over UFPLA structures. Since DMMP decomposition does not obviously depend on the partial pressure of O₂, we did not consider the O₂ species in model analysis.

Scheme 1 shows the primary reaction steps in the Langmuir-Hinshelwood model for DMMP decomposition in the presence of DMMP and H₂O reactants over the UFPLA catalysts. The reaction involves quasi-equilibrated DMMP adsorption on surface site (*). leading to formation of DMMP* species (step 1). Similarly, quasiequilibrated adsorption of H2O on active site (*) results in H2O* species (step 2). The reaction between adsorbed DMMP* and H₂O* forms adsorbed methylphosphonate (MMP*) and methanol (step 3), which is the rate limiting step (RLS) of the reaction network. Since the kinetics data were collected from the first 10% disappearance of the starting reactant, the effects of reaction intermediates or products on the initial decomposition kinetics can be ignored. Therefore, the contribution of reaction step 4 and the following steps, for instance, decomposition from methylphosphonate to further products, were excluded from the model in the rate equation derivation. Under pseudo-steady state assumption for adsorbed DMMP* and H_2O^* species, the rate equation for DMMP decomposition (r_{DMMP} , mol s⁻¹) is shown in Eq. (1):

$$r_{DMMP} = \frac{k_3 K_1 K_2 p_{DMMP} p_{H_2O} \theta_{total}^2}{(1 + K_1 p_{DMMP} + K_2 p_{H_2O})^2}$$
(1)

where k_3 (mol [mol Ti]⁻² s⁻¹) is DMMP decomposition rate constant in step 3; K_1 (Pa⁻¹) and K_2 (Pa⁻¹) are the equilibrium constants for the adsorption of DMMP (step 1) and H_2O (step 2), respectively; p_{DMMP} (Pa) and p_{H_2O} (Pa) are the partial pressures of DMMP and H_2O ; θ_{total} (mol Ti) is the total Ti element in the UFPLA catalyst. Details on the rate equation derivations can be referred to section S4 in the Supporting Information.

Scheme 2 shows the proposed primary reaction steps for DMMP decomposition over the UFPLA catalysts following the Eley-Rideal model. The reaction involved quasi-equilibrated DMMP

Step (1): DMMP +
$$* \stackrel{K_1}{\leftrightarrow} DMMP^*$$

Step (2): DMMP* + $H_2O \stackrel{k_2}{\rightarrow} MMP^* + CH_3OH (RLS)$
Step (3): MMP* $\stackrel{K_3}{\leftrightarrow} MMP + *$

Scheme 2. Elementary steps in Eley-Rideal reaction model in photocatalytic DMMP decomposition.

adsorption on surface site (*) to form DMMP* species (step 1). The reaction between H_2O vapor and molecularly adsorbed DMMP* forms MMP* (step 2, RLS). Under pseudo-steady state assumption for DMMP* species and negligible contribution of reaction intermediates and final products, the rate equation for DMMP consumption (r_{DMMP} , mol s^{-1}) is shown in Eq. (2):

$$r_{\text{DMMP}} = \frac{k_2 K_1 p_{\text{DMMP}} p_{\text{H}_2\text{O}} \theta_{\text{total}}}{1 + K_1 p_{\text{DMMP}}}$$
 (2)

where K_1 (Pa⁻¹) is the equilibrium constant for the adsorption of DMMP (step 1) and k_2 (mol [mol Ti]⁻¹ s⁻¹ Pa⁻¹) is DMMP decomposition rate constant in step 2. Section S5 in the Supporting Information details the derivation of this rate equation.

The kinetic parameters in Eq. (1) were analyzed from the kinetics data in Fig. 4. When $p_{\rm H_2O}$ is fixed and p_{DMMP} is the variable, Eq. (1) can be linearized as,

$$\sqrt{\frac{p_{\text{DMMP}}}{r_{\text{DMMP}}}} = \frac{K_1 p_{\text{DMMP}}}{\sqrt{k_3 K_1 K_2 p_{\text{H}_2O}} \theta_{\text{total}}} + \frac{1 + K_2 p_{\text{H}_2O}}{\sqrt{k_3 K_1 K_2 p_{\text{H}_2O}} \theta_{\text{total}}}$$
(3)

where the slope (defined as S_1) is, $S_1 = \frac{K_1}{\sqrt{k_3 K_1 K_2 p_{H_2} o \theta_{total}}}$, and the intercept (denoted as I_1) is $I_1 = \frac{1 + K_2 p_{H_2} o}{\sqrt{k_3 K_1 K_2 p_{H_2} o \theta_{total}}}$. Similarly, when p_{DMMP} is fixed in the experiment, the linear form of Eq. (1) is,

$$\sqrt{\frac{p_{\rm H_2O}}{r_{\rm DMMP}}} = \frac{K_2 p_{\rm H_2O}}{\sqrt{k_3 K_1 K_2 p_{\rm DMMP}} \theta_{\rm total}} + \frac{1 + K_1 p_{\rm DMMP}}{\sqrt{k_3 K_1 K_2 p_{\rm DMMP}} \theta_{\rm total}}$$
(4)

in which the slope (defined as S_2) and intercept (denoted as I_2) are $S_2 = \frac{K_2}{\sqrt{k_3 K_1 K_2 p_{DMMP} \theta_{total}}}$ and $I_2 = \frac{1 + K_1 p_{DMMP}}{\sqrt{k_3 K_1 K_2 p_{DMMP} \theta_{total}}}$, respectively. The ratio of S_1/S_2 gives Eq. (5),

$$S_1/S_2 = \frac{K_1}{K_2} \sqrt{\frac{p_{\text{DMMP}}}{p_{\text{H}_2\text{O}}}}$$
 (5)

The ratio of I_1/I_2 is,

$$I_1/I_2 = \frac{1 + K_2 p_{H_2O}}{1 + K_1 p_{DMMP}} \sqrt{\frac{p_{DMMP}}{p_{H_2O}}}$$
 (6)

Fig. 5 shows the linearized correlations of $\sqrt{\frac{p_{\rm DMMP}}{r_{\rm DMMP}}}$ versus $p_{\rm DMMP}$ (Fig. 5a) and $\sqrt{\frac{p_{\rm H_2O}}{r_{\rm DMMP}}}$ versus $p_{\rm H_2O}$ (Fig. 5b), respectively, by re-plotting

(Fig. 5a) and $\sqrt{\frac{PH_2O}{PDMP}}$ versus p_{H_2O} (Fig. 5b), respectively, by re-plotting the kinetics data in Fig. 4a—b using Eqs. (3) and (4), respectively. The linear fitting with coefficient of determination (R^2) > 0.9, positive intercept and slope in each set of kinetic data supports the proposed Langmuir-Hinshelwood model for fitting the DMMP decomposition on the UFPLA structure. From Eqs. (5) and (6), the adsorption equilibrium constants K_1 and K_2 were evaluated to be $2.93 \times 10^{-2} \, \text{Pa}^{-1}$ and $1.45 \times 10^{-3} \, \text{Pa}^{-1}$, respectively. The adsorption equilibrium constant reflects the bound nature of reaction species on the UFPLA catalyst. Apparently, DMMP has stronger adsorption

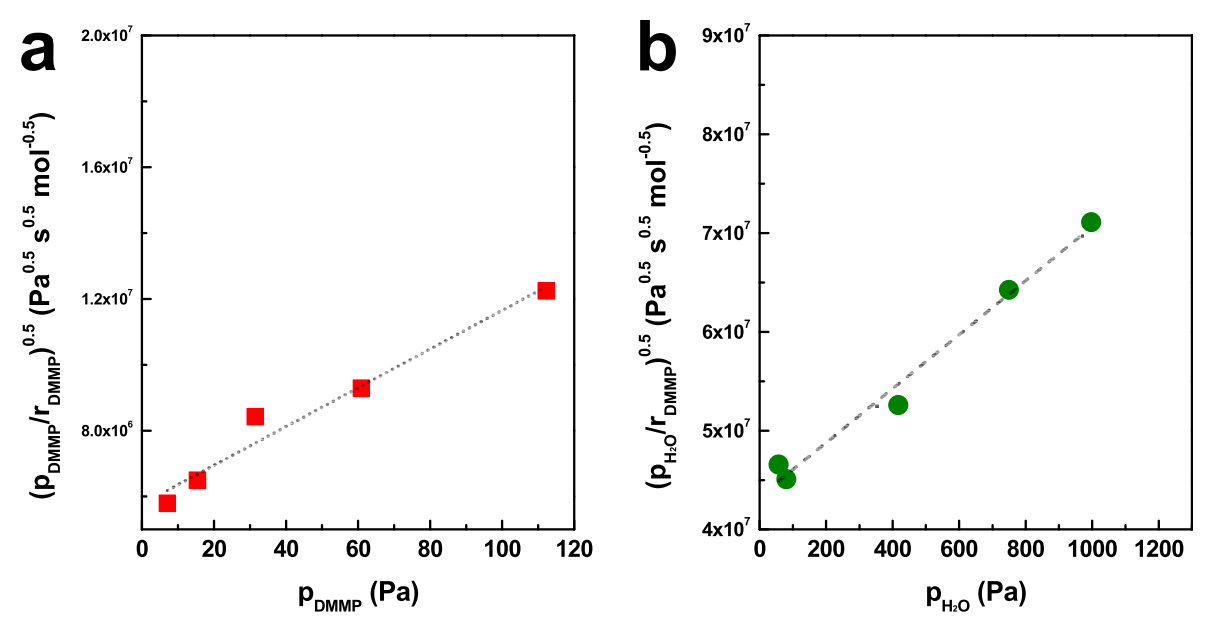


Fig. 5. Linearized correlations of $\sqrt{\frac{p_{\rm DMMP}}{r_{\rm DMMP}}}$ versus $p_{\rm DMMP}$ (a) and $\sqrt{\frac{p_{\rm H_2O}}{r_{\rm DMMP}}}$ versus $p_{\rm H_2O}$ (b) for DMMP decomposition over the 12-nm-TiO₂ UFPLA.

on the catalyst than that of H_2O . By substituting K_1 and K_2 into the slope (S_1), the reaction rate constant (k_3) can be calculated as 24.48 mol [mol Ti]⁻² s⁻¹.

To examine the fitting of the Eley-Rideal model for the DMMP decomposition kinetics, the rate law for DMMP consumption (r_{DMMP} , mol s⁻¹) is shown in Eq. (7):

$$r_{\text{DMMP}} = \frac{k_2 K_1 p_{\text{DMMP}} p_{\text{H}_2\text{O}} \theta_{\text{total}}}{1 + K_1 p_{\text{DMMP}}}$$
 (7)

where k_2 (mol s^{-1} Pa^{-1} [mol Ti]⁻¹) is the rate constant of DMMP decomposition.

When $p_{\rm H_2O}$ is fixed and p_{DMMP} is the variable, Eq. (7) can be linearized as follows,

$$\frac{1}{r_{DMMP}} = \frac{1}{k_2 K_1 p_{DMMP} p_{H_2O} \theta_{total}} + \frac{1}{k_2 p_{H_2O} \theta_{total}}$$
 (8)

where the slope (defined as S_1 ') is S_1 ' = $\frac{1}{k_2 K_1 p_{H_20} \theta_{total}}$, and the intercept (denoted as I_1 ') is I_1 ' = $\frac{1}{k_2 p_{H_20} \theta_{total}}$. Similarly, when p_{DMMP} is fixed in the experiment, the linear form of Eq. (7) is,

$$r_{\text{DMMP}} = \frac{k_2 K_1 p_{\text{DMMP}} \theta_{\text{total}}}{1 + K_1 p_{\text{DMMP}}} p_{\text{H}_2\text{O}}$$
(9)

From Eq. (9), the DMMP decomposition rate (r_{DMMP}) should increase linearly with increasing p_{H_2O} and the intercept should be

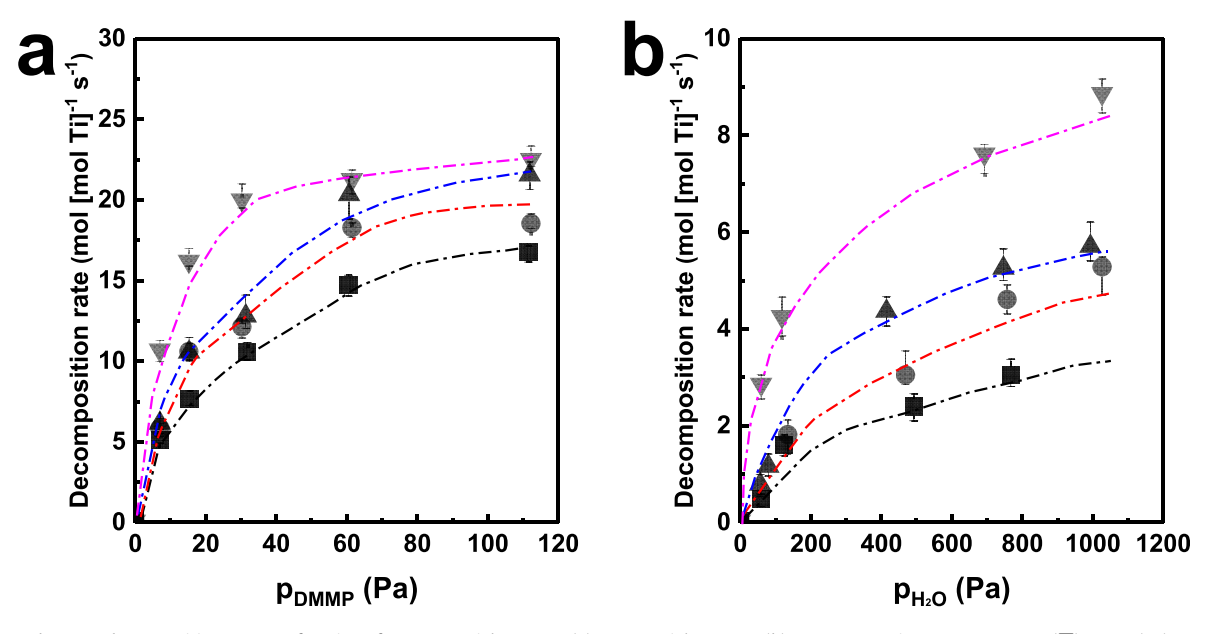


Fig. 6. Measured DMMP decomposition rate as a function of DMMP partial pressure (a), H₂O partial pressure (b) over 12-nm-TiO₂ UFPLA at 293 K (), 333 K () and 348 K () (Reaction conditions in Fig. 6a: 1.19 kPa H₂O pressure, 17.02 kPa O₂ pressure, 5 h reaction time; Reaction conditions in Fig. 6b: 7.09 Pa DMMP pressure, 4.28 kPa O₂ pressure, 5 h reaction time).

Table 1Kinetic parameters obtained from the Langmuir-Hinshelwood model used for analysis of DMMP decomposition kinetics over the 12-nm-thick TiO₂ UFPLA catalyst.

Temperature (K)	293	313	333	348
$K_1^{a} (Pa^{-1})$ $K_2^{b} (Pa^{-1})$	$\begin{array}{c} 1.28 \times 10^{-2} \\ 6.71 \times 10^{-4} \end{array}$	$\begin{array}{c} 2.04 \times 10^{-2} \\ 6.96 \times 10^{-4} \end{array}$	$\begin{array}{c} 2.38 \times 10^{-2} \\ 8.55 \times 10^{-4} \end{array}$	$6.23\times 10^{-2}\\2.04\times 10^{-3}$
$k_3^{\ c}$ (mol [mol Ti] ⁻² s ⁻¹)	17.18	26.86	33.68	36.97

^a Equilibrium constant of DMMP adsorption.

zero. This trend conflicts with the experimental data shown in Fig. 4b, which shows the Langmuir correlation between DMMP decomposition rate and partial pressure of water. Therefore, the Eley-Rideal model cannot describe the observed kinetics.

3.3.3. Effect of reaction temperature on DMMP decomposition

To further understand the performance of UFPLA in DMMP decomposition, we examined the effect of reaction temperature, ranging from 293 K to 348 K, on the decomposition kinetics. As shown in Fig. 6a, the photocatalytic DMMP decomposition increases with increasing reaction temperature for each set of partial pressures of p_{DMMP} . Similarly, the increase in reaction temperature speeds up the decomposition of DMMP at each partial pressure of $p_{\rm H_2O}$ (Fig. 6b). From the Langmuir-Hinshelwood model and the linearized rate equations (Eqs. (3) and (4)), the adsorption equilibrium constants (K_1 and K_2) and the reaction rate constant (k_3) at each reaction temperature are evaluated, and the results are summarized in Table 1. Detailed kinetics analysis following the Langmuir-Hinshelwood model is included in Section S7 in the Supporting Information. It shows that the equilibrium constants of DMMP adsorption (K_1) and water adsorption (K_2) proportionally increased with increasing reaction temperature. At all tested temperatures, K₁ is always higher than K₂, which reflects the DMMP has a stronger adsorption on the UFPLA catalyst. The DMMP decomposition rate constant (k_3) also increases with the increase in the reaction. This is consistent with the faster DMMP decomposition rate at a higher reaction temperature condition.

4. Conclusions

The ultrathin-film photocatalytic light absorber (UFPLA) were studied for the first time for the photocatalytic DMMP decomposition. The UFPLA structure is comprised of a TiO₂ thin-film and an Al reflector, sequentially deposited on a supportive glass substrate. The nanocavity effect of the structure improves optical absorption in ultra-thin TiO2 films, and thus maintains strong light absorption and charge carrier extraction efficiency for efficient photocatalytic DMMP decomposition. Compared to the commercial Aeroxide®P25 catalyst, an enhancement of 2013-fold in DMMP decomposition rate was achieved on the TiO₂/Al UFPLA with 12-nm thick TiO₂ film. The dependence of DMMP decompositions on the reactant pressure and reaction temperature over the 12-nm-TiO₂ thin-film UFPLA were examined. The collected decomposition kinetics can be interpreted by the Langmuir-Hinshelwood model. The initial kinetic parameters were analyzed based on the Langmuir-Hinshelwood model, which can guide further understanding on DMMP decomposition behavior over the new UFPLA structures.

Declaration of competing interest

The authors declare that they have no known competing financial interests or personal relationships that could have appeared to influence the work reported in this paper.

Acknowledgements

This material is based upon work supported by, or in part by, the U. S. Army Research Laboratory and the U. S. Army Research Office under contract/grant number: W911NF-17-1-0363. The authors gratefully acknowledge financial support from National Science Foundation (NSF-CBET 1264599 and NSF-CBET 1351384).

Appendix A. Supplementary data

Supplementary data to this article can be found online at https://doi.org/10.1016/j.chemosphere.2021.129719.

Author contributions

Wei Wu did the majority of the experiments including reactor assembly, catalysis tests and kinetic model development and analysis. Haomin Song measured the morphology and optical properties of the catalyst structures. Wei Wu and Dongxia Liu did data discussion and contributed to the manuscript writing. Qiaoqiang Gan and Dongxia Liu supervised the project.

References

Ahmed, S.N., Haider, W., 2018. Heterogeneous photocatalysis and its potential applications in water and wastewater treatment: a review. Nanotechnology 29, 342001

Alexander, D.A., Klein, S., 2006. The challenge of preparation for a chemical, biological, radiological or nuclear terrorist attack. J. Postgrad. Med. 52, 126–131.

Aprile, C., Corma, A., Garcia, H., 2008. Enhancement of the photocatalytic activity of TiO₂ through spatial structuring and particle size control: from subnanometric to submillimetric length scale. Phys. Chem. Chem. Phys. 10, 769–783.

Blanco-Galvez, J., Fernández-Ibáñez, P., Malato-Rodríguez, S., 2006. Solar photocatalytic detoxification and disinfection of water: recent overview. J. Sol. Energy Eng. 129, 4–15.

Dalrymple, O.K., Stefanakos, E., Trotz, M.A., Goswami, D.Y., 2010. A review of the mechanisms and modeling of photocatalytic disinfection. Appl. Catal., B 98, 27–38.

De Laat, J., Boudiaf, N., Dossier-Berne, F., 2010. Effect of dissolved oxygen on the photodecomposition of monochloramine and dichloramine in aqueous solution by UV irradiation at 253.7 nm. Water Res. 44, 3261–3269.

Dotan, H., Kfir, O., Sharlin, E., Blank, O., Gross, M., Dumchin, I., Ankonina, G., Rothschild, A., 2013. Resonant light trapping in ultrathin films for water splitting. Nat. Mater. 12. 158–164.

Echavia, G.R.M., Matzusawa, F., Negishi, N., 2009. Photocatalytic degradation of organophosphate and phosphonoglycine pesticides using TiO₂ immobilized on silica gel. Chemosphere 76, 595–600.

Fagan, R., McCormack, D.E., Dionysiou, D.D., Pillai, S.C., 2016. A review of solar and visible light active TiO₂ photocatalysis for treating bacteria, cyanotoxins and contaminants of emerging concern. Mater. Sci. Semicond. Process. 42, 2–14.

Fujishima, A., Zhang, X., Tryk, D.A., 2008. TiO₂ photocatalysis and related surface phenomena. Surf. Sci. Rep. 63, 515–582.

Grätzel, C.K., Jirousek, M., Grätzel, M., 1990. Decomposition of organophosphorus compounds on photoactivated ${\rm TiO_2}$ surfaces. J. Mol. Catal. 60, 375–387.

Habisreutinger, S.N., Schmidt-Mende, L., Stolarczyk, J.K., 2013. Photocatalytic reduction of CO₂ on TiO₂ and other semiconductors. Angew. Chem. Int. Ed. 52, 7372–7408

Hirakawa, T., Nosaka, Y., 2002. Properties of O₂⁻ and OH[•] formed in TiO₂ aqueous suspensions by photocatalytic reaction and the influence of H₂O₂ and some ions. Langmuir 18, 3247–3254.

Janisch, C., Song, H., Zhou, C., Lin, Z., Elías, A.L., Ji, D., Terrones, M., Gan, Q., Liu, Z., 2016. MoS₂ monolayers on nanocavities: enhancement in light—matter interaction. 2D Mater. 3, 025017.

b equilibrium constant of water adsorption.

^c rate constant of DMMP decomposition.

Jun, Y., Park, J.H., Kang, M.G., 2012. The preparation of highly ordered TiO₂ nanotube Arrays by an anodization method and their applications. Chem. Commun. 48, 6456–6471.

- Kabra, K., Chaudhary, R., Sawhney, R.L., 2004. Treatment of hazardous organic and inorganic compounds through aqueous-phase photocatalysis: a review. Ind. Eng. Chem. Res. 43, 7683–7696.
- Kamat, P.V., 2007. Meeting the clean energy demand: nanostructure architectures for solar energy conversion. J. Phys. Chem. C 111, 2834–2860.
- Kats, M.A., Blanchard, R., Genevet, P., Capasso, F., 2013. Nanometre optical coatings based on strong interference effects in highly absorbing media. Nat. Mater. 12, 20–24.
- Kitano, M., Matsuoka, M., Ueshima, M., Anpo, M., 2007. Recent developments in titanium oxide-based photocatalysts. Appl. Catal., A 325, 1–14.
- Knudson, G.B., 2001. Nuclear, biological, and chemical training in the US army reserves: mitigating psychological consequences of weapons of mass destruction. Mil. Med. 166. 63–65.
- Konstantinou, I.K., Sakellarides, T.M., Sakkas, V.A., Albanis, T.A., 2001. Photocatalytic degradation of selected s-triazine herbicides and organophosphorus insecticides over aqueous TiO₂ suspensions. Environ. Sci. Technol. 35, 398–405.
- secticides over aqueous TiO₂ suspensions. Environ. Sci. Technol. 35, 398–405. Kozlova, E.A., Smirniotis, P.G., Vorontsov, A.V., 2004. Comparative study on photocatalytic oxidation of four organophosphorus simulants of chemical warfare agents in aqueous suspension of titanium dioxide. J. Photochem. Photobiol., A 162, 503–511.
- Krosley, K.W., Collard, D.M., Adamson, J., Fox, M.A., 1993. Degradation of organophosphonic acids catalyzed by irradiated titanium dioxide. J. Photochem. Photobiol., A 69, 357–360.
- Kumar, S.G., Devi, L.G., 2011. Review on modified TiO₂ photocatalysis under UV/ visible light: selected results and related mechanisms on interfacial charge carrier transfer dynamics. J. Phys. Chem. 115, 13211–13241.
- Kusior, A., Radecka, M., Zakrzewska, K., Reszka, A., Kowalski, B., 2013. Sensitization of TiO₂/SnO₂ nanocomposites for gas detection. Sensor. Actuator. B Chem. 189, 251–259
- Lan, Y., Lu, Y., Ren, Z., 2013. Mini review on photocatalysis of titanium dioxide nanoparticles and their solar applications. Nanomater. Energy 2, 1031–1045.
- Liang, Y.T., Vijayan, B.K., Lyandres, O., Gray, K.A., Hersam, M.C., 2012. Effect of dimensionality on the photocatalytic behavior of carbon—titania nanosheet composites: charge transfer at nanomaterial interfaces. J. Phys. Chem. Lett. 3, 1760—1765.
- Linsebigler, A.L., Lu, G., Yates Jr., J.T., 1995. Photocatalysis on TiO₂ surfaces: principles, mechanisms, and selected results. Chem. Rev. 95, 735–758.
- Liu, E., Qi, L., Bian, J., Chen, Y., Hu, X., Fan, J., Liu, H., Zhu, C., Wang, Q., 2015. A facile strategy to fabricate plasmonic Cu modified TiO₂ nano-flower films for photocatalytic reduction of CO₂ to methanol. Mater. Res. Bull. 68, 203–209.
- Liu, L., Chen, X.B., 2014. Titanium dioxide nanomaterials: self-structural modifications. Chem. Rev. 114, 9890—9918.
- Liu, Y., Li, Z., Green, M., Just, M., Li, Y.Y., Chen, X., 2017. Titanium dioxide nanomaterials for photocatalysis. J. Phys. D Appl. Phys. 50, 193003.

Ma, Y., Wang, X.L., Jia, Y.S., Chen, X.B., Han, H.X., Li, C., 2014. Titanium dioxide-based nanomaterials for photocatalytic fuel generations. Chem. Rev. 114, 9987–10043.

- MatouŠEk, J., 2006. Health and environmental threats associated with the destruction of chemical weapons. Ann. N. Y. Acad. Sci. 1076, 549–558.
- Mengyue, Z., Shifu, C., Yaowu, T., 1995. Photocatalytic degradation of organophosphorus pesticides using thin films of TiO₂. J. Chem. Technol. Biotechnol. 64, 339–344.
- Mergel, D., 2001. Modeling thin TiO₂ films of various densities as an effective optical medium. Thin Solid Films 397. 216–222.
- Mor, G.K., Varghese, O.K., Paulose, M., Shankar, K., Grimes, C.A., 2006. A review on highly ordered, vertically oriented TiO₂ nanotube Arrays: fabrication, material properties, and solar energy applications. Sol. Energy Mater. Sol. Cells 90, 2011–2075.
- Moss, J.A., Szczepankiewicz, S.H., Park, E., Hoffmann, M.R., 2005. Adsorption and photodegradation of dimethyl methylphosphonate vapor at TiO₂ surfaces. J. Phys. Chem. B 109, 19779—19785.
- O'Shea, K.E., Garcia, I., Aguilar, M., 1997. TiO₂ photocatalytic degradation of dimethyl- and diethyl- methylphosphonate, effects of catalyst and environmental factors. Res. Chem. Intermed. 23, 325–339.
- Obee, T.N., Satyapal, S., 1998. Photocatalytic decomposition of DMMP on titania. J. Photochem. Photobiol., A 118, 45–51.
- Robertson, P.K., Bahnemann, D.W., Robertson, J.M., Wood, F., 2005. Photocatalytic detoxification of water and air. In: Boule, P., Bahnemann, D.W., Robertson, P.K.J. (Eds.), Environmental Photochemistry Part II. Springer, Berlin, Heidelberg, pp. 367–423.
- Schneider, J., Matsuoka, M., Takeuchi, M., Zhang, J., Horiuchi, Y., Anpo, M., Bahnemann, D.W., 2014. Understanding TiO₂ photocatalysis: mechanisms and materials. Chem. Rev. 114, 9919–9986.
- Song, H., Guo, L., Liu, Z., Liu, K., Zeng, X., Ji, D., Zhang, N., Hu, H., Jiang, S., Gan, Q., 2014. Nanocavity enhancement for ultra-thin film optical absorber. Adv. Mater. 26, 2737–2743.
- Song, H., Wu, W., Liang, J.-W., Maity, P., Shu, Y., Wang, N.S., Mohammed, O.F., Ooi, B.S., Gan, Q., Liu, D., 2018. Ultrathin-film titania photocatalyst on nanocavity for CO₂ reduction with boosted catalytic efficiencies. Global Challenges 2, 1800032
- Talmage, S.S., Watson, A.P., Hauschild, V., Munro, N.B., King, J., 2007. Chemical warfare agent degradation and decontamination. Curr. Org. Chem. 11, 285–298.
- Tetyana, V., Yekaterina, D., Mykola, K., 2006. Alleviation of toxic impact of chemical agents on human organism. In: Dishovsky, C., Pivovarov, A., Benschop, H. (Eds.), Medical Treatment of Intoxications and Decontamination of Chemical Agent in the Area of Terrorist Attack. Springer, Dordrecht, pp. 191–201.
- Thakur, R.S., Chaudhary, R., Singh, C., 2010. Fundamentals and applications of the photocatalytic treatment for the removal of industrial organic pollutants and effects of operational parameters: a review. J. Renew. Sustain. Energy 2, 042701.
- Xia, Z., Song, H., Kim, M., Zhou, M., Chang, T.-H., Liu, D., Yin, X., Xiong, K., Mi, H., Wang, X., Xia, F., Yu, Z., Ma, Z., Gan, Q., 2017. Single-crystalline germanium nanomembrane photodetectors on foreign nanocavities. Sci. Adv. 3, e1602783.